

SIMBIG: A Forward Modeling Approach To Analyzing Galaxy Clustering

ChangHoon Hahn^{a,1}, Michael Eickenberg^b, Shirley Ho^c, Jiamin Hou^{d,e}, Pablo Lemos^{f, g, c}, Elena Massara^{h,i}, Chirag Modi^{b, c}, Azadeh Moradinezhad Dizgah^j, Bruno Régaldo-Saint Blancard^b, and Muntazir M. Abidi^j

^aDepartment of Astrophysical Sciences, Princeton University, Princeton NJ 08544, USA; ^bCenter for Computational Mathematics, Flatiron Institute, 162 5th Ave, New York, NY 10010, USA; ^cCenter for Computational Astrophysics, Flatiron Institute, 162 5th Ave 5th floor, New York, NY 10010, USA; ^dDepartment of Astronomy, University of Florida, 211 Bryant Space Science Center, Gainesville, FL 32611, USA; ^eMax-Planck-Institut für Extraterrestrische Physik, Postfach 1312, Giessenbachstrasse 1, 85748 Garching bei München, Germany; ^fDepartment of Physics, Université de Montréal, Montréal, 1375 Avenue Thérèse-Lavoie-Roux, QC H2V 0B3, Canada; ^gMila - Quebec Artificial Intelligence Institute, Montréal, 6666 Rue Saint-Urbain, QC H2S 3H1, Canada; ^hWaterloo Centre for Astrophysics, University of Waterloo, 200 University Ave W, Waterloo, ON N2L 3G1, Canada; ⁱDepartment of Physics and Astronomy, University of Waterloo, 200 University Ave W, Waterloo, ON N2L 3G1, Canada; ^jDépartement de Physique Théorique, Université de Genève, 24 quai Ernest Ansermet, 1211 Genève 4, Switzerland

This manuscript was compiled on November 3, 2022

We present the first-ever cosmological constraints from a simulation-based inference (SBI) analysis of galaxy clustering from the new SIMBIG forward modeling framework. SIMBIG leverages the predictive power of high-fidelity simulations and provides an inference framework that can extract cosmological information on small non-linear scales, inaccessible with standard analyses. In this work, we apply SIMBIG to the BOSS CMASS galaxy sample and analyze the power spectrum, $P_\ell(k)$, to $k_{\text{max}} = 0.5 h/\text{Mpc}$. We construct 20,000 simulated galaxy samples using our forward model, which is based on high-resolution QUIJOTE N -body simulations and includes detailed survey realism for a more complete treatment of observational systematics. We then conduct SBI by training normalizing flows using the simulated samples and infer the posterior distribution of ΛCDM cosmological parameters: $\Omega_m, \Omega_b, h, n_s, \sigma_8$. We derive significant constraints on Ω_m and σ_8 , which are consistent with previous works. Our constraints on σ_8 are 27% more precise than standard analyses. This improvement is equivalent to the statistical gain expected from analyzing a galaxy sample that is $\sim 60\%$ larger than CMASS with standard methods. It results from additional cosmological information on non-linear scales beyond the limit of current analytic models, $k > 0.25 h/\text{Mpc}$. While we focus on P_ℓ in this work for validation and comparison to the literature, SIMBIG provides a framework for analyzing galaxy clustering using any summary statistic. We expect further improvements on cosmological constraints from subsequent SIMBIG analyses of summary statistics beyond P_ℓ .

cosmology | machine learning | galaxies | simulation

The three-dimensional spatial distribution of galaxies provides key cosmological information that can be used to constrain the nature of dark matter and dark energy and measure the contents of the Universe. The next generation spectroscopic galaxy surveys, conducted using the Dark Energy Spectroscopic Instrument (DESI; 1–3), Subaru Prime Focus Spectrograph (PFS; 4, 5), the ESA *Euclid* satellite mission (6), and the Nancy Gracy Roman Space Telescope (Roman; 7, 8), will probe galaxies over unprecedented cosmic volumes out to $z \sim 3$, over 10 Gyrs of cosmic history. Combined with other cosmological probes, they will provide the most stringent tests of the standard ΛCDM cosmological model and potentially lead to discoveries of new physics.

In current analyses, the power spectrum is used as the primary measurement of galaxy clustering (e.g. 9–11). Furthermore, the analyses are limited to large, linear scales where the impact of non-linear structure formation is small. These restrictions result from the fact that standard analyses use

analytic models based on perturbation theory (PT) of large-scale structure (see 12, 13, for a review). PT struggles to accurately model scales beyond quasi-linear scales, especially for higher-order clustering statistics (e.g. bispectrum). In the (14) PT analysis, for instance, the authors restrict the power spectrum to $k < 0.2 h/\text{Mpc}$ and the bispectrum to $k < 0.08 h/\text{Mpc}$. In a recent PT analysis, (15) analyzes the bispectrum to $k < 0.23 h/\text{Mpc}$; however, they require 33 extra parameters for the theoretical consistency of their model. PT also cannot be used to model various newly proposed summary statistics (e.g. 16) or to exploit the full galaxy distribution at the field level.

Another major challenge for current analyses is accurately accounting for observational systematics. Observations suffer from imperfections in e.g. targeting, imaging, completeness that can significantly impact the analysis (17, 18). Current analyses account for these effects by applying correction weights to the galaxies. Fiber collisions, for example, prevent galaxy surveys that use fiber-fed spectrographs (e.g. DESI, PFS) from successfully measuring redshifts from galaxies within some angular scale of one another on the focal plane. This significantly biases the power spectrum by more

Significance Statement

The three-dimensional spatial distribution of galaxies encodes key cosmological information on the nature of dark energy and the contents of the Universe. Current analyses of the statistical clustering of galaxies successfully extract information on large scales that are well described by analytic models. They, however, struggle on smaller, non-linear, scales. Here we present SIMBIG, a new approach to galaxy clustering analyses that can extract information on non-linear regimes by exploiting high-fidelity simulations and inference based on machine learning. To demonstrate its advantages, we apply SIMBIG to 109,636 galaxies of the BOSS survey and analyze a standard summary statistic of the galaxy distribution. Our constraints are consistent with previous works and substantially improve their precision on select cosmological parameters.

C.H., M.E., S.H., P.L., E.M., A.M.D., B.R.B., and M.A. designed research; C.H. performed research; C.H., M.E., S.H., J.H., P.L., E.M., A.M.D., and B.R.B. contributed new reagents/analytic tools; C.H., M.E., S.H., J.H., P.L., E.M., C.M., A.M.D., and B.R.B. analyzed data; and C.H., M.E., S.H., J.H., P.L., E.M., C.M., A.M.D., and B.R.B. wrote the paper.

The authors declare no conflict of interest.

¹changhoon.hahn@princeton.edu

than the amplitude of cosmic variance on scales smaller than $k > 0.1 h/\text{Mpc}$ (19–21). To correct for this effect, the weights of the “collided” galaxies missed by survey are assigned to their nearest angular neighbors (22, 23). Even for current analyses, these correction weights do not sufficiently correct the measured power spectrum (20). Furthermore, they are only designed and demonstrated for the power spectrum.

Meanwhile, additional cosmological information is available on non-linear scales and in higher-order statistics. Recent studies have accurately quantified the information content in these regimes using large suites of simulations. (24) and (25) used the QUIJOTE suite of simulations to demonstrate that constraints on cosmological parameters, $\Omega_m, \Omega_b, h, n_s, \sigma_8$, improve by a factor of ~ 2 by including non-linear scales ($0.2 < k < 0.5 h/\text{Mpc}$) in power spectrum analyses. Even more improvement comes from including higher-order clustering information in the bispectrum. Similar forecasts for other summary statistics, *e.g.* marked power spectrum (26, 27), reconstructed power spectrum (28), skew spectra (29), wavelet statistics (30), find consistent improvements from including non-linear scales and higher-order clustering. Despite the growing evidence of the significant constraining power available in non-linear scales and higher-order statistics, it cannot be exploited by standard methods with PT.

Robustly exploiting non-linear and non-Gaussian cosmological information requires a framework that can both accurately model non-linear structure formation and account for detailed observational systematics. In this work, we present SIMulation-Based Inference of Galaxies (SIMBIG), a framework for analyzing galaxy clustering that achieves these requirements by using a forward modeling approach. Instead of analyzing galaxy clustering using analytic models, a forward model approach uses simulations that model the full details of the observations.

In SIMBIG, our forward model is based on cosmological N -body simulations that accurately models non-linear structure formation. We also use the halo occupation framework, which provides a compact and flexible prescription for connecting the galaxy distribution to the dark matter distribution. Our forward model also takes advantage of the fact that many observational systematics can be more easily included in simulations (*e.g.* 31, 32) than corrected in the observations. With this forward model, we can rigorously analyze galaxy clustering on non-linear scales and with higher-order statistics.

To infer the cosmological parameters, our approach does not require sampling the posterior using an assumed analytic likelihood. We instead use simulation-based inference (SBI; see 33, for a review). SBI, also known as “likelihood-free inference”, enables accurate Bayesian inference using forward models (*e.g.* 34–37). Moreover, they leverage neural density estimation from machine learning (*e.g.* 34, 38) to more efficiently infer the posterior without sampling or making strong assumptions on the functional form of the likelihood.

In this work, we apply SIMBIG to the CMASS galaxy sample observed by the Sloan Digital Sky Survey SDSS-III Baryon Oscillation Spectroscopic Survey (BOSS; 39, 40). With the main goal of demonstrating the accuracy and potential of SIMBIG, we use the power spectrum as our summary statistic. We present the cosmological constraints inferred from our analysis and compare them to previous constraints in the literature. In an accompanying paper (41, hereafter H22b), we present our forward model in further detail and the mock

challenge that we conduct to rigorously validate the accuracy of SIMBIG cosmological constraints.

Simulation-Based Inference of Galaxies SIMBIG

Modern cosmological analyses use Bayesian inference to constrain the posterior distribution $p(\boldsymbol{\theta} | \boldsymbol{x})$ of cosmological parameters, $\boldsymbol{\theta}$, given observation \boldsymbol{x} . In standard galaxy clustering analyses, the posterior is evaluated using Bayes’ rule. The likelihood is assumed to have a Gaussian functional form and evaluated using an analytic PT model.

SBI offers an alternative that requires no assumptions on the form of the likelihood. SBI only requires a forward model, *i.e.* a simulation to generate mock observations \boldsymbol{x}' given parameters $\boldsymbol{\theta}'$. It uses a training dataset of simulated pairs $(\boldsymbol{\theta}', \boldsymbol{x}')$ to estimate the posterior. SBI has already been successfully applied to a wide range of inference problems in astronomy and cosmology (35, 36, 42–47).

In this work, we utilize SBI based on neural density estimation, where a neural network q with parameters ϕ is trained to estimate $p(\boldsymbol{\theta} | \boldsymbol{x}) \approx q_\phi(\boldsymbol{\theta} | \boldsymbol{x})$. In particular, we use “normalizing flow” models that are capable of accurately estimating complex distributions (48, 49). Below, we briefly describe our forward model and SBI framework.

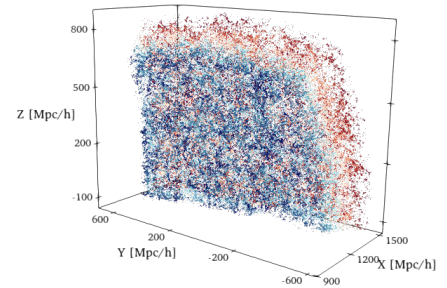
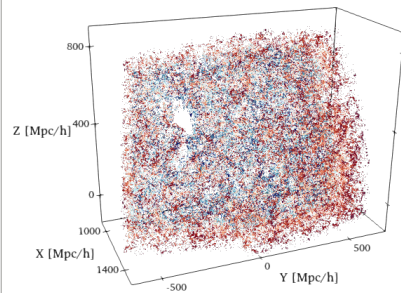
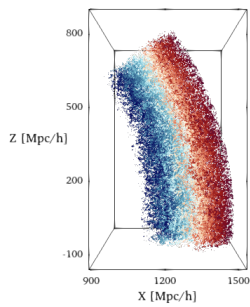
A. Forward Model. SBI requires a forward model that is capable of generating mock observations which are statistically indistinguishable from the observations. We start with high-resolution N -body simulations from the QUIJOTE suite (50). These simulations follow the evolution of 1024^3 cold dark matter (CDM) particles in a volume of $(1 h^{-1} \text{Gpc})^3$ from $z = 127$ to $z = 0.5$ using the TreePM GADGET-III code. They accurately model the clustering of matter down to non-linear scales beyond $k = 0.5 h/\text{Mpc}$ (50).

To model the galaxy distribution, we identify gravitationally bound dark matter halos and populate them with galaxies using a flexible halo occupation framework. We identify halos using the ROCKSTAR phase-space-based halo finder (51), which accurately determines the location of halos and resolves their substructure (52). We then populate the halos using Halo Occupation Distribution (HOD) models that provide a statistical prescription for populating halos with galaxies based on halo properties such as their mass and concentration. In this work, we use a state-of-the-art HOD model that supplements the standard (53) model with assembly, concentration, and velocity biases. The extra features of our HOD model add additional flexibility that recent works suggest may be necessary to describe galaxy clustering (*e.g.* 54–56).

Once we have our galaxy distribution in the simulation box, we apply survey realism. We remap the box to a cuboid (57) and then cut out the detailed survey geometry of the BOSS CMASS SGC sample (see Materials and Methods). This includes masking for bright stars, centerpost, bad field, and collision priority (17, 18, 40). We apply fiber collisions by first identifying all pairs of galaxies within an angular scale of $62''$ then, for 60% of the pairs, removing one of the galaxies from the sample. Lastly, we trim the forward modeled galaxy catalog to match the $0.45 < z < 0.6$ redshift range and angular range of the observations.

In total, our forward model has 14 parameters. 5 Λ CDM cosmological parameters, $\Omega_m, \Omega_b, h, n_s, \sigma_8$, that determine the matter distribution and 9 HOD parameters that determine the

CMASS SGC



SimBIG Forward Model

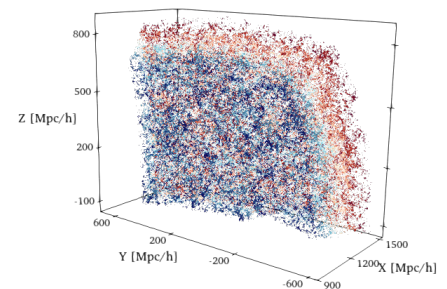
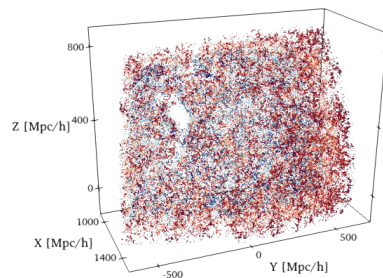
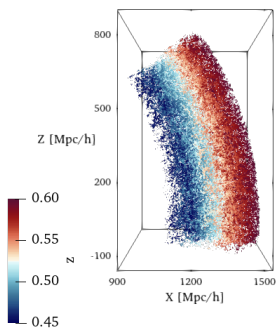


Fig. 1. The SIMBIG forward model produces simulated galaxy samples with the same survey geometry and observational systematics as the observed BOSS CMASS SGC galaxy sample. We present the 3D distribution of the galaxies from three different viewing angles. The colormap represents the redshift of the galaxies. In the top set of panels, we present the distribution of galaxies in the CMASS sample. In the bottom, we present the distribution of a simulated galaxy sample, generated from our forward model. The SIMBIG galaxy samples are constructed from QUIJOTE N -body dark matter simulations using an HOD model that populates dark matter halos identified using the ROCKSTAR algorithm. The 3D distributions illustrate that our forward model is able to generate galaxy distributions that are difficult to statistically distinguish from observations. For more comparisons of the 3D distributions, we refer readers to [1](#).

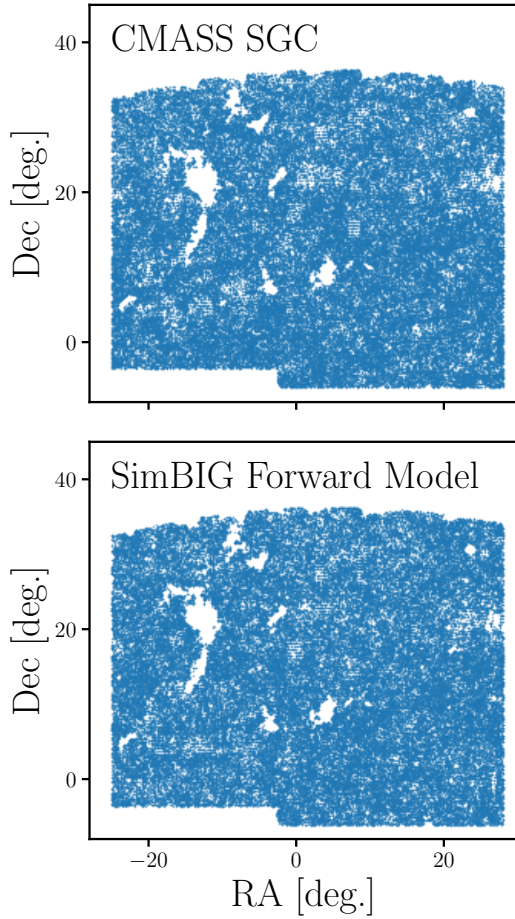


Fig. 2. Angular distribution of galaxies from the CMASS sample (top) and a galaxy sample generated using the SIMBIG forward model (bottom). Comparison of the angular distributions highlights the detailed CMASS angular selection that we include in our forward model to account for observational systematics.

connection between galaxies and halos. For further details on our forward model, we refer readers to H22b. In the bottom panels of Fig. 1, we present the three-dimensional spatial distribution of galaxies in our forward model. We present the angular distribution of galaxies in our forward model in Fig. 2. The forward model accurately reproduces the survey geometry and angular footprint of the observed BOSS sample. For additional comparisons of the 3D distributions of galaxies in CMASS and our forward model, we refer readers to [🌐*](#).

B. Training Dataset for Simulation-Based Inference. Using our forward model, we construct 20,000 simulated galaxy catalogs. They are constructed from 2,000 QUIJOTE N -body simulations with 10 different sets of HOD parameters, sampled from a broad prior. The N -body simulations are arranged in a Latin Hypercube configuration, which therefore imposes uniform priors on the cosmological parameters that conservatively encompasses the *Planck* cosmological constraints (58).

In principle, SIMBIG can be directly applied to the full galaxy catalog if the forward model is capable of accurately modeling observations at all scales. Even with N -body simulations, however, this is not the case due to limitations on

mass and time resolution and inadequacies of halo occupation models. Instead, we use summary statistics of the galaxy sample, where we can impose cuts, *e.g.*, based on physical scales, to which our forward model is accurate. Since the primary goal of this work is to present and demonstrate the SIMBIG framework, we use the most commonly used summary statistic: the galaxy power spectrum multipole, $P_\ell(k)$. We also include the average galaxy number density of the sample, \bar{n}_g .

In this work, we use the redshift-space galaxy power spectrum monopole, quadrupole, and hexadecapole ($\ell = 0, 2$, and 4). We measure P_0 , P_2 , and P_4 for each of the simulated galaxy catalogs using the (59) algorithm. In this work, we impose a conservative $k < k_{\max} = 0.5 h/\text{Mpc}$ limit on the P_ℓ , based on the convergence of matter clustering of the QUIJOTE simulations (see H22b for further details). We also measure the power spectrum for the BOSS CMASS-SGC galaxy sample with the same algorithm. For the observed $\hat{P}_\ell(k)$ we include systematics weights for redshift failures, stellar density, and seeing conditions, which are effects not included in our forward model but shown to be successfully accounted for using the weights (17, 23).

By using P_ℓ , we can compare the constraints inferred using SIMBIG with previous constraints (*e.g.* 10, 11) as further validation of SIMBIG. To be further consistent with previous analyses, we include a nuisance parameter, A_{shot} , that is typically included to account for residual shot noise contribution (*e.g.* 9–11). In Fig. 3, we present $P_\ell(k)$ of our forward modeled galaxy catalogs. We randomly select 100 out of the total 20,000 power spectra for clarity. The left, center, and right panels present the monopole, quadrupole, and hexadecapole. These P_ℓ measurements and \bar{n}_g serve as the training dataset $\{(\theta', \mathbf{x}')\}$ for our SBI posterior estimation using normalizing flows.

C. Simulation-Based Inference with Normalizing Flows. Normalizing flow models use an invertible bijective transformation, $f : \mathbf{z} \mapsto \theta$, to map a complex target distribution to a simple base distribution, $\pi(\mathbf{z})$, that is fast to evaluate. For SBI, the target distribution is the posterior, $p(\theta|\mathbf{x})$ while $\pi(\mathbf{z})$ is typically a multivariate Gaussian. The transformation f must be invertible and have a tractable Jacobian so that we can evaluate the target distribution from $\pi(\mathbf{z})$ by change of variables. Since $\pi(\mathbf{z})$ is easy to sample and evaluate, we can also easily sample and evaluate the target distribution. A neural network with parameters ϕ is trained to obtain f .

Among the various normalizing flow-based neural density estimators now available in the literature, we use a Masked Autoregressive Flow (MAF; 34). MAF combines normalizing flows with an autoregressive design (60), which is well-suited for estimating conditional probability distributions such as a posterior. A MAF model is built by stacking multiple Masked Autoencoder for Distribution Estimation (MADE; 38) models so that it has the autoregressive structure of MADE models but with additional flexibility to describe complex probability distributions. We use the MAF implementation of the `sbi` Python package (61, 62).

In training, our goal is to determine the parameters, ϕ , of our normalizing flow, $q_\phi(\theta|\mathbf{x})$, so that it accurately estimates the posterior, $p(\theta|\mathbf{x})$. We can formulate this into an optimization problem of minimizing the Kullback-Leibler (KL) divergence between $p(\theta, \mathbf{x}) = p(\theta|\mathbf{x})p(\mathbf{x})$ and $q_\phi(\theta|\mathbf{x})p(\mathbf{x})$,

*<https://youtube.com/playlist?list=PLQk8Faa2x0twK3fgs55ednnHD2vblzo4z>

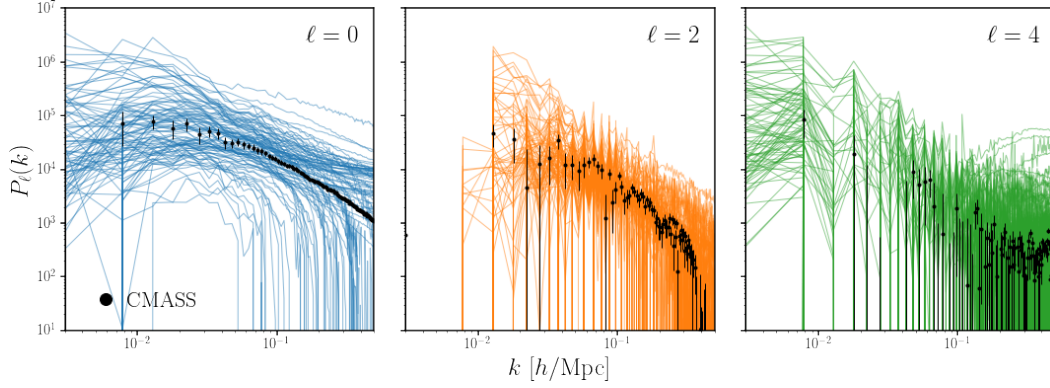


Fig. 3. Power spectrum, $P_\ell(k)$, measured from the simulated galaxy catalogs constructed using the SIMBIG forward model. We present $P_\ell(k)$ of 100 out of the total 20,000 catalogs for clarity. In each of the panels, we plot the monopole, quadrupole, and hexadecapole of the power spectrum ($\ell = 0, 2, 4$). For reference, we include $P_\ell(k)$ measured from the BOSS CMASS SGC galaxy sample (black) with uncertainties estimated from H22b simulations. P_ℓ is the most commonly used summary statistic of galaxy distribution that measures the two-point clustering. We use P_ℓ in this work to showcase and validate the SIMBIG framework and make detailed comparisons to previous works in the literature. The P_ℓ of the SIMBIG catalogs encompass the BOSS P_ℓ and, thus, provide a sufficiently broad dataset to conduct SBI.

which measures the difference between the two distributions.

$$\begin{aligned} \min_{\phi} D_{\text{KL}}(p(\theta, \mathbf{x}) \parallel q_{\phi}(\theta | \mathbf{x})p(\mathbf{x})) \\ &= \min_{\phi} \int p(\theta, \mathbf{x}) \log \frac{p(\theta | \mathbf{x})}{q_{\phi}(\theta | \mathbf{x})} d\theta d\mathbf{x} \quad [1] \\ &\approx \min_{\phi} \sum_i \log p(\theta_i | \mathbf{x}_i) - \log q_{\phi}(\theta_i | \mathbf{x}_i) \quad [2] \\ &\approx \min_{\phi} \sum_i -\log q_{\phi}(\theta_i | \mathbf{x}_i) \quad [3] \\ &\approx \max_{\phi} \sum_i \log q_{\phi}(\theta_i | \mathbf{x}_i). \quad [4] \end{aligned}$$

Eq. 2 follows from the fact that the training dataset $\{(\theta', \mathbf{x}')\}$ is constructed by sampling from $p(\theta, \mathbf{x})$ with our forward model.

We split the training data into a training and validation set with a 90/10 split, then maximize Eq. 4 over the training set. We use the ADAM optimizer (63) with a learning rate of 5×10^{-4} . We prevent overfitting by stopping the training when the log-likelihood (Eq. 4) evaluated on the validation set fails to increase after 20 epochs. We determine the architecture of our normalizing flow through experimentation. Our final trained model has 6 MADE blocks, each with 9 hidden layers and 186 hidden units. For further details on the training procedure, we refer readers to H22b. Once trained, we estimate the posterior of our 5 cosmological, 9 HOD parameters, and 1 nuisance parameter. for the BOSS CMASS SGC \hat{P}_ℓ and \hat{n}_g , by sampling our normalizing flow $q_{\phi}(\theta | \hat{\mathbf{x}})$.

1. Results

We present the posterior distribution of the Λ CDM cosmological parameters, $\Omega_m, \Omega_b, h, n_s, \sigma_8$, inferred from $P_\ell(k)$ using SIMBIG in Fig. 4. The posterior is inferred from the BOSS $P_\ell(k)$ down to $k_{\text{max}} = 0.5 h/\text{Mpc}$. The diagonal panels present the marginalized one-dimensional posteriors for each parameter. The other panels present marginalized two-dimensional posteriors of different parameter pairs that highlight parameter degeneracies. We mark the 68 and 95 percentiles of the posteriors with the contours. We infer the posterior of HOD

and nuisance parameters; however, we do not include them in the figure for clarity. Among the cosmological parameters, the SIMBIG posterior significantly constrains Ω_m and σ_8 . This is consistent with previous works that relied on priors from Big Bang nucleosynthesis or cosmic microwave background (CMB) experiments for the other parameters, Ω_b and n_s (e.g. 10, 11). We infer $\Omega_m = 0.292^{+0.055}_{-0.040}$ and $\sigma_8 = 0.812^{+0.067}_{-0.068}$.

In the accompanying paper H22b, we present the validation of the SIMBIG posterior using a suite of 1,500 test simulations. We construct the test suite using different forward models than the one used for our training data. They are constructed using different N -body simulations, halo finders, and HOD models. This is to ensure that the cosmological constraints we derive are independent of the choices and assumptions made in our forward model.

For validation, we conduct a mock challenge where we infer posteriors of the cosmological parameters for each of the test simulations. Since we know the true cosmological parameter values of the test simulations, we can access the accuracy and precision of the inferred posteriors. H22b reveals that SIMBIG produces unbiased posteriors. On the other hand, the posteriors are conservative, *i.e.* they are broader than the true posterior. This is due to the limited number of N -body simulations used to construct our training dataset, which makes the estimate of the KL divergence (Eq. 2) noisy. Our constraint on Ω_m is particularly conservative. Additional N -body simulations would significantly improve the precision of our posteriors.

Despite the fact that they are conservative, the σ_8 posterior from SIMBIG is significantly more precise than constraints from previous works. (10) analyzed the P_ℓ of the BOSS CMASS galaxy sample using the PT approach with an analytic model based on effective field theory. For the CMASS SGC sample, with uniform priors on the cosmological parameters, and with $k_{\text{max}} = 0.25 h/\text{Mpc}$, (10) inferred $\sigma_8 = 0.719^{+0.100}_{-0.085}$. With SIMBIG, we improve σ_8 constraints by 27% over the standard galaxy clustering analysis. We emphasize that this improvement is roughly equivalent to analyzing a galaxy survey $\sim 60\%$ larger than the original survey using PT.

Recently, (11) also analyzed the P_ℓ of BOSS CMASS sample

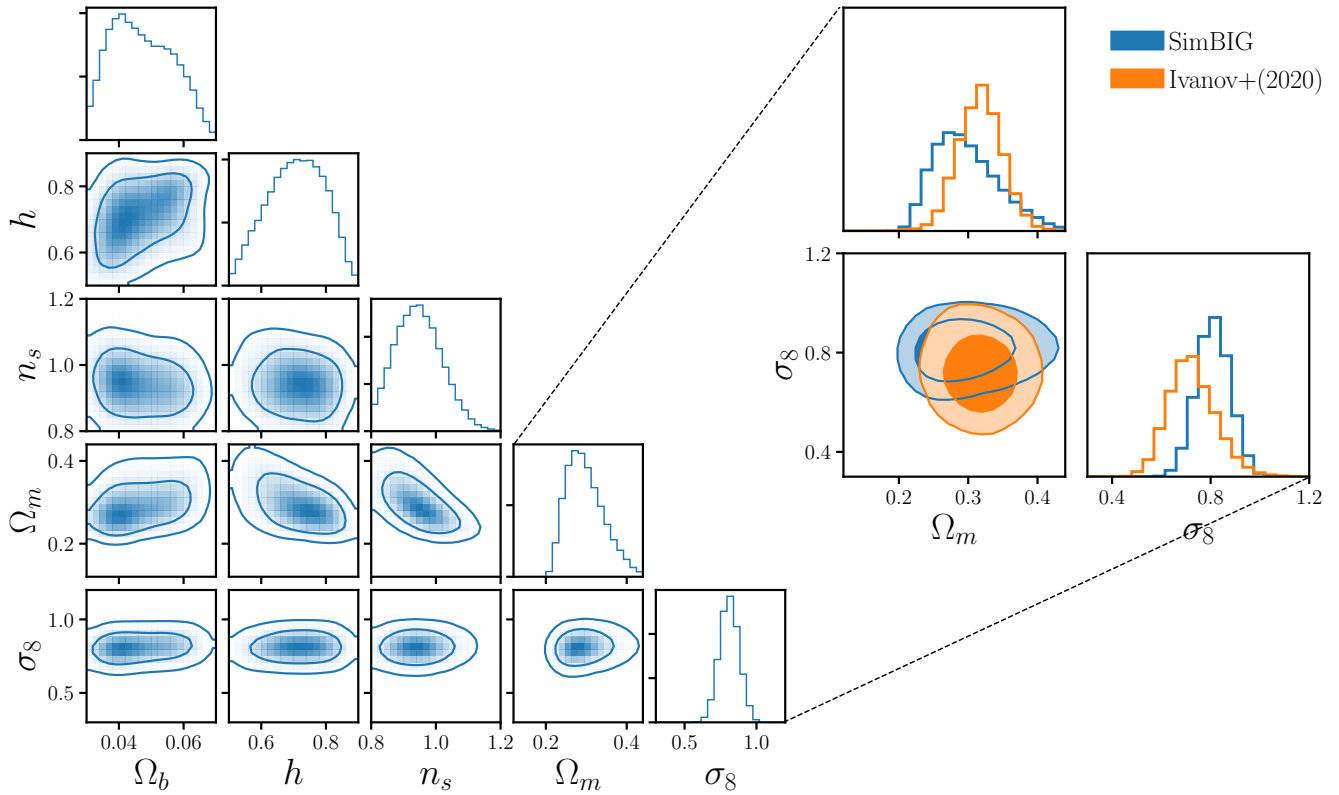


Fig. 4. *Left:* Posterior of cosmological parameters inferred from P_ℓ using SIMBIG. In the diagonal panels we present the marginalized 1D posterior of each parameter. The other panels present the 2D posteriors that illustrate the degeneracies between two parameters. The contours mark the 68 and 95 percentiles. We accurately analyze P_ℓ down to non-linear regimes, $k_{\text{max}} = 0.5 h/\text{Mpc}$, by using a simulation-based forward model that includes observational systematics. *Right:* We focus on the posteriors of (Ω_m , σ_8), the parameters that can be most significantly constrained by galaxy clustering alone. We derive $\Omega_m = 0.292^{+0.055}_{-0.040}$ and $\sigma_8 = 0.812^{+0.067}_{-0.068}$. Our σ_8 constraints are 27% tighter than the (10) $k_{\text{max}} = 0.25 h/\text{Mpc}$ PT constraint (orange).

but using a theoretical model based on a halo power spectrum emulator. Instead of using a galaxy bias scheme used by PT to connect the galaxy and matter distributions, (11) used halo power spectra predicted by an emulator and a halo occupation framework, similar to the HOD model in our forward model. We note that while the halo power spectrum emulator is trained using simulations, the approach in (11) does not forward model observational systematics. They also make the same assumptions on the form of the likelihood as PT analyses for their inference. For the CMASS SGC sample, with uniform priors on all cosmological parameters, and with $k_{\max} = 0.25 h/\text{Mpc}$, (11) inferred $\sigma_8 = 0.790^{+0.083}_{-0.072}$. The (11) constraints are tighter than the (10) PT constraints because the halo occupation model provides a more compact framework for modeling galaxies. Nevertheless, with SIMBIG, we improve on their σ_8 constraints by 13%.

SIMBIG produces significantly tighter constraints on σ_8 because we are able to accurately extract cosmological information available on small, non-linear, scales. With our forward modeling approach, we can accurately model non-linear clustering and robustly account for observational systematics down to $k_{\max} = 0.5 h/\text{Mpc}$. In both (10) and (11), they restrict their analysis to $k_{\max} < 0.25 h/\text{Mpc}$ due to the limitations of their analyses on smaller scales.

To further verify that our improvement comes from constraining power at $k > 0.25 h/\text{Mpc}$, we analyze P_ℓ to $k_{\max} = 0.25 h/\text{Mpc}$ using SIMBIG. In Fig. 5, we present the SIMBIG $k_{\max} = 0.25 h/\text{Mpc}$ posterior (blue) along with the posteriors from (10, orange) and (11, green). We focus our comparison on Ω_m and σ_8 , the cosmological parameters that can be most competitively constrained with galaxy clustering alone. The contours again represent the 68 and 95 percentiles. We find overall good agreement among the posteriors. All of the posteriors are statistically consistent with each other. For σ_8 , our $k_{\max} = 0.25 h/\text{Mpc}$ places a $\sigma_8 = 0.861^{+0.070}_{-0.091}$ constraint. This is significantly broader than our $k_{\max} = 0.5 h/\text{Mpc}$ constraint, which demonstrates that the constraining power is in fact from non-linear scales. Furthermore, the precision of the $k_{\max} = 0.25 h/\text{Mpc}$ SIMBIG constraint is in excellent agreement with the (11) constraint. This serves as further validation of SIMBIG, since (11) uses a similar halo occupation framework to model the power spectrum.

For Ω_m , we infer broader posteriors than (10) and (11). As we discuss in H22b, this is due to the fact that the SIMBIG normalizing flow is trained using a limited number of simulations. We use 20,000 forward modeled simulations; however, they are constructed from 2000 N -body simulations with different values of cosmological parameters. To estimate the expected improvement in the Ω_m constraints, we use the posterior ‘‘re-calibration’’ procedure from (64). The re-calibration uses the posteriors inferred for the test simulations and their true parameter values. We calculate the local probability integral transform (65), a diagnostic of the inferred posteriors, and use this quantity to derive a weighting scheme that corrects the posteriors so that it matches the true posterior of the test simulations.

The re-calibration uses test simulations, so we do not use it for inference. However, it provides a bound for the SIMBIG constraints if we were to have sufficient training simulations. The re-calibrated posterior constrains $\Omega_m = 0.284^{+0.021}_{-0.017}$. For reference, we mark the re-calibrated Ω_m constraint (black

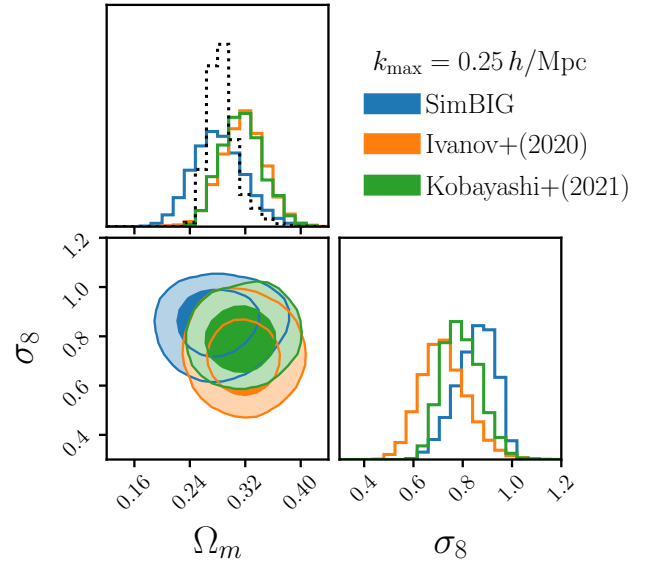


Fig. 5. Comparison of the (Ω_m, σ_8) posteriors inferred from the P_ℓ CMASS-SGC analysis for $k_{\max} = 0.25 h/\text{Mpc}$ from SIMBIG (blue), the (10) PT approach (orange), and the (11) emulator approach (green). The contours represent the 68 and 95 percentiles. We find overall good agreement among the posteriors. For Ω_m , SIMBIG infers consistent but broader posterior due to the fact that we use a limited number of simulations. We estimate the expected Ω_m constraints with more simulations using posterior ‘‘re-calibration’’ (black dotted). For σ_8 , both SIMBIG and (11) derive tighter constraints than (10) due to the fact that we use halo occupation instead of a galaxy bias prescription. Meanwhile, the precision of our σ_8 constraint is in excellent agreement with (11), which uses a similar halo occupation model. The consistency of the $k_{\max} = 0.25 h/\text{Mpc}$ posteriors demonstrate that the improvements in the $k_{\max} = 0.5 h/\text{Mpc}$ constraints come from additional cosmological information in the non-linear regime that SIMBIG can robustly extract.

dotted) in Fig. 5. The re-calibrated Ω_m is in good agreement with both the (10) and (11) constraints. It is significantly tighter than the original SIMBIG constraint and illustrates that additional training simulations would significantly improve the precision of the SIMBIG Ω_m constraints.

Based on our $k_{\max} = 0.5 h/\text{Mpc}$ posterior, we infer $S_8 = \sigma_8 \sqrt{\Omega_m}/0.3 = 0.802^{+0.102}_{-0.092}$ (and $0.797^{+0.078}_{-0.076}$ for our re-calibrated posterior). Multiple recent large-scale structure studies have reported a ‘‘ S_8 tension’’ with constraints from the (58) CMB analysis. They find significantly lower values of S_8 than *Planck* (66–73). PT analyses of BOSS also infer relatively low values of S_8 . (10), for instance, infers $S_8 = 0.737^{+0.110}_{-0.092}$. This S_8 tension between constraints from large-scale structure and CMB analyses has motivated a number of works to explore modifications of the standard Λ CDM cosmological model (*e.g.* 74–77). We do not find a significant S_8 tension with the *Planck* constraints (58). However, given the statistical precision of our S_8 constraint, we refrain from more detailed comparison and discussion.

2. Conclusions

We present SIMBIG, a forward modeling framework for analyzing galaxy clustering using SBI. As a demonstration of the framework, we apply it to the BOSS CMASS SGC, a galaxy sample at $z \sim 0.5$. We analyze the galaxy power spectrum multipoles (P_ℓ), the most commonly used summary statistic of the galaxy spatial distribution, to showcase and validate the SIMBIG framework.

SIMBIG utilizes a full forward model of the CMASS sample, unlike standard approaches that use analytic models of the summary statistic. The forward model is based on high-resolution QUIJOTE N -body simulations that can accurately model the matter distribution on small scales. It uses halo modeling and a state-of-the-art HOD model with assembly, concentration, and velocity biases that provide a flexible mapping between the matter and galaxy distributions. The forward model also includes realistic observational systematics such as survey geometry and fiber collisions. With this forward modeling approach, we can leverage the predictive power of simulations to analyze small, non-linear, scales as well as higher-order clustering. It also provides a framework to account for systematics for any summary statistic.

Using the forward model, we construct 20,000 simulated CMASS-like samples that span a wide range of cosmological and HOD parameters. We measure P_ℓ and \bar{n}_g for each of these samples and use the measurements as the training dataset for SBI. To estimate the posterior, we use neural density estimation based on normalizing flows. Using the training dataset, we train our normalizing flows by minimizing the KL divergence between its posterior estimate and the true posterior. Once trained, we apply our normalizing flow to the observed summary statistics to infer the posterior of 5 cosmological, 9 HOD, and 1 nuisance parameter.

Focusing on the cosmological parameters, we derive significant constraints on: $\Omega_m = 0.316^{+0.040}_{-0.036}$ and $\sigma_8 = 0.668^{+0.0324}_{-0.0284}$. Our σ_8 constraints are 27% tighter than the (10) constraints using a standard PT approach on the same galaxy sample. This improvement is roughly equivalent to increasing the volume of the galaxy survey by $\sim 60\%$ for a standard PT analysis. The SIMBIG constraints are inferred from P_ℓ out to $k_{\max} = 0.5 h/\text{Mpc}$ while the PT constraints are limited to $k_{\max} = 0.25 h/\text{Mpc}$. The improvement is driven by the additional cosmological information on non-linear scales that SIMBIG can robustly extract.

We also infer the posterior using SIMBIG from P_ℓ with $k_{\max} = 0.25 h/\text{Mpc}$ and compare it to posteriors in the literature. In particular, the SIMBIG σ_8 constraint for $k_{\max} = 0.25 h/\text{Mpc}$ are in excellent agreement with the constraint from the recent halo model based emulator analysis of (11). Since they use a similar halo occupation framework as SIMBIG, this comparison firmly verifies the robustness of our constraints. The comparison also confirms that the improvement in SIMBIG $k_{\max} = 0.5 h/\text{Mpc}$ constraints come from the non-linear regime. In the accompanying H22b, we present additional tests of SIMBIG through a mock challenge. The tests use a suite of 1,500 test simulations constructed with different forward models to demonstrate that SIMBIG produces unbiased cosmological constraints. H22b also presents further details on our forward model and discusses posterior constraints on HOD parameters.

SIMBIG can also extract higher-order cosmological information. Standard galaxy clustering analyses primarily focus on two-point clustering statistics. Analyses of higher-order statistics have been limited to, *e.g.* the bispectrum (14, 15, 78), and even these analyses extract only limited cosmological information beyond linear scales. In subsequent work, we will use SIMBIG to analyse the BOSS CMASS galaxies using higher-order statistics (the bispectrum) and non-standard observables that contain additional cosmological information: *e.g.* marked

power spectrum, skew spectra, void probability functions, and wavelet-scattering-like statistics. We will also apply SIMBIG to analyze field-level summary statistics that capture all the information in the galaxy field using convolutional and graph neural networks.

SIMBIG can also be extended to upcoming spectroscopic galaxy surveys observed using DESI, PFS, *Euclid*, and *Roman* will probe unprecedented cosmic volumes over the next decade. They will produce the largest and most detailed three-dimensional maps of galaxies in the Universe. These surveys are already expected to provide the most precise constraints on cosmological parameters using standard analyses. SIMBIG can further exploit the statistical power of these surveys to place even tighter constraints on cosmological parameters and produce the most stringent tests of the standard Λ CDM cosmological model and beyond.

Materials and Methods

Observations: SDSS-III BOSS. In this work, we analyze observations from the Sloan Digital Sky Survey SDSS-III (39, 40) Baryon Oscillation Spectroscopic Survey (BOSS) Data Release 12. In particular, we use the CMASS galaxy sample, which selects high stellar mass Luminous Red Galaxies (LRGs) over the redshift $0.43 < z < 0.7$ (79). We restrict our analysis to CMASS galaxies in the Southern Galactic Cap (SGC) and impose a redshift cut of $0.45 < z < 0.6$ and the following angular cuts: $\text{Dec} > -6$ and $-25 < \text{RA} < 28$. In upper panels in Fig. 1, we present the three-dimensional distributions of our CMASS SGC galaxy sample at three different viewing angles. We also present the angular distribution of the sample in Fig. 2. In total, our CMASS SGC galaxy sample contains 109,636 galaxies.

ACKNOWLEDGMENTS. It is a pleasure to thank Peter Melchior, Uroš Seljak, David Spergel, Licia Verde, and Benjamin D. Wandelt for valuable discussions. We also thank Mikhail M. Ivanov and Yosuke Kobayashi for providing us with the posteriors used in the comparison. This work was supported by the AI Accelerator program of the Schmidt Futures Foundation. This work was also supported by NASA ROSES grant 12-EUCLID12-0004 NASA grant 15-WFIRST15-0008. JH has received funding from the European Union's Horizon 2020 research and innovation program under the Marie Skłodowska-Curie grant agreement No 101025187. AMD acknowledges funding from Tomalla Foundation for Research in Gravity and Boninchi Foundation.

1. D Collaboration, et al., The DESI Experiment Part I: Science, Targeting, and Survey Design. *arXiv:1611.00036 [astro-ph]* (2016).
2. D Collaboration, et al., The DESI Experiment Part II: Instrument Design. *arXiv:1611.00037 [astro-ph]* (2016).
3. B Abareshi, et al., Overview of the Instrumentation for the Dark Energy Spectroscopic Instrument (2022).
4. M Takada, et al., Extragalactic science, cosmology, and Galactic archaeology with the Subaru Prime Focus Spectrograph. *Publ. Astron. Soc. Jpn.* **66**, R1 (2014).
5. N Tamura, et al., Prime Focus Spectrograph (PFS) for the Subaru telescope: Overview, recent progress, and future perspectives in *Ground-Based and Airborne Instrumentation for Astronomy VI*. (eprint: arXiv:1608.01075), Vol. 9908, p. 99081M (2016).
6. R Laureijs, et al., Euclid Definition Study Report. *arXiv e-prints* p. arXiv:1110.3193 (2011).
7. D Spergel, et al., Wide-Field Infrared Survey Telescope-Astrophysics Focused Telescope Assets WFIRST-AFTA 2015 Report (2015).
8. Y Wang, et al., The High Latitude Spectroscopic Survey on the Nancy Grace Roman Space Telescope. *The Astrophys. J.* **928**, 1 (2022).
9. F Beutler, et al., The clustering of galaxies in the completed SDSS-III Baryon Oscillation Spectroscopic Survey: Anisotropic galaxy clustering in Fourier space. *Mon. Notices Royal Astron. Soc.* **466**, 2242–2260 (2017).
10. MM Ivanov, M Simonović, M Zaldarriaga, Cosmological parameters from the BOSS galaxy power spectrum. *J. Cosmol. Astropart. Phys.* **2020**, 042 (2020).
11. Y Kobayashi, T Nishimichi, M Takada, H Miyatake, Full-shape cosmology analysis of SDSS-III BOSS galaxy power spectrum using emulator-based halo model: A 5% determination of σ_8 . *arXiv:2110.06969 [astro-ph]* (2021).

12. F Bernardeau, S Colombi, E Gaztanaga, R Scoccimarro, Large-Scale Structure of the Universe and Cosmological Perturbation Theory. *Phys. Reports* **367**, 1–248 (2002).
13. V Desjacques, D Jeong, F Schmidt, Large-Scale Galaxy Bias. *arXiv:1611.09787 [astro-ph, physics:gr-qc, physics:hep-ph]* (2016).
14. OHE Philcox, MM Ivanov, The BOSS DR12 Full-Shape Cosmology: Λ CDM Constraints from the Large-Scale Galaxy Power Spectrum and Bispectrum Monopole. *arXiv:2112.04515 [astro-ph, physics:hep-ex]* (2021).
15. G D'Amico, Y Donath, M Lewandowski, L Senatore, P Zhang, The BOSS bispectrum analysis at one loop from the Effective Field Theory of Large-Scale Structure (2022).
16. K Naidoo, E Massara, O Lahav, Cosmology and neutrino mass with the Minimum Spanning Tree. *Mon. Notices Royal Astron. Soc.* (2022).
17. AJ Ross, et al., The clustering of galaxies in the SDSS-III Baryon Oscillation Spectroscopic Survey: Analysis of potential systematics. *Mon. Notices Royal Astron. Soc.* **424**, 564–590 (2012).
18. AJ Ross, et al., The clustering of galaxies in the completed SDSS-III Baryon Oscillation Spectroscopic Survey: Observational systematics and baryon acoustic oscillations in the correlation function. *Mon. Notices Royal Astron. Soc.* **464**, 1168–1191 (2017).
19. H Guo, I Zehavi, Z Zheng, A New Method to Correct for Fiber Collisions in Galaxy Two-point Statistics. *The Astrophys. J.* **756**, 127 (2012).
20. C Hahn, R Scoccimarro, MR Blanton, JL Tinker, SA Rodríguez-Torres, The Effect of Fiber Collisions on the Galaxy Power Spectrum Multipoles. *Mon. Notices Royal Astron. Soc.* **467**, 1940–1956 (2017).
21. D Bianchi, et al., Unbiased clustering estimates with the DESI fibre assignment. *Mon. Notices Royal Astron. Soc.* **481**, 2338–2348 (2018).
22. I Zehavi, et al., Galaxy Clustering in Early Sloan Digital Sky Survey Redshift Data. *The Astrophys. J.* **571**, 172–190 (2002).
23. L Anderson, et al., The clustering of galaxies in the SDSS-III Baryon Oscillation Spectroscopic Survey: Baryon acoustic oscillations in the Data Releases 10 and 11 Galaxy samples. *Mon. Notices Royal Astron. Soc.* **441**, 24–62 (2014).
24. C Hahn, F Villaescusa-Navarro, E Castorina, R Scoccimarro, Constraining M_V with the bispectrum. Part I. Breaking parameter degeneracies. *J. Cosmol. Astropart. Phys.* **03**, 040 (2020).
25. C Hahn, F Villaescusa-Navarro, Constraining M_V with the bispectrum. Part II. The information content of the galaxy bispectrum monopole. *J. Cosmol. Astropart. Phys.* **2021**, 029 (2021).
26. E Massara, F Villaescusa-Navarro, S Ho, N Dalal, DN Spergel, Using the Marked Power Spectrum to Detect the Signature of Neutrinos in Large-Scale Structure. *arXiv:2001.11024 [astro-ph]* (2020).
27. E Massara, et al., Cosmological Information in the Marked Power Spectrum of the Galaxy Field (2022).
28. Y Wang, et al., Extracting high-order cosmological information in galaxy surveys with power spectra (2022).
29. J Hou, A Moradinezhad Dizgah, C Hahn, E Massara, Cosmological Information in Skew Spectra of Biased Tracers in Redshift Space. *arXiv e-prints* p. arXiv:2210.12743 (2022).
30. M Eickenberg, et al., Wavelet Moments for Cosmological Parameter Estimation (2022).
31. SA Rodríguez-Torres, et al., The clustering of galaxies in the SDSS-III Baryon Oscillation Spectroscopic Survey: Modelling the clustering and halo occupation distribution of BOSS CMASS galaxies in the Final Data Release. *Mon. Notices Royal Astron. Soc.* **460**, 1173–1187 (2016).
32. G Rossi, et al., The Completed SDSS-IV Extended Baryon Oscillation Spectroscopic Survey: N-body Mock Challenge for Galaxy Clustering Measurements. *Mon. Notices Royal Astron. Soc.* **505**, 377–407 (2021).
33. K Cranmer, J Brehmer, G Louppe, The frontier of simulation-based inference. *Proc. Natl. Acad. Sci.* **117**, 30055–30062 (2020).
34. G Papamakarios, T Pavlakou, I Murray, Masked Autoregressive Flow for Density Estimation. *arXiv e-prints* **1705**, arXiv:1705.07057 (2017).
35. J Alsing, T Charnock, S Feeney, B Wandelt, Fast likelihood-free cosmology with neural density estimators and active learning. *Mon. Notices Royal Astron. Soc.* **488**, 4440–4458 (2019).
36. N Jeffrey, J Alsing, F Lanusse, Likelihood-free inference with neural compression of DES SV weak lensing map statistics. *Mon. Notices Royal Astron. Soc.* **501**, 954–969 (2021).
37. L Tortorelli, et al., The PAU Survey: Measurement of Narrow-band galaxy properties with Approximate Bayesian Computation. *arXiv:2106.02651 [astro-ph]* (2021).
38. M Germain, K Gregor, I Murray, H Larochele, MADE: Masked Autoencoder for Distribution Estimation. *Proc. 32nd Int. Conf. on Mach. Learn.* **37**, 881–889 (2015).
39. DJ Eisenstein, et al., SDSS-III: Massive Spectroscopic Surveys of the Distant Universe, the Milky Way, and Extra-Solar Planetary Systems. *The Astron. J.* **142**, 72 (2011).
40. KS Dawson, et al., The Baryon Oscillation Spectroscopic Survey of SDSS-III. *The Astron. J.* **145**, 10 (2013).
41. C Hahn, et al., SIMBIG: Mock Challenge for a Forward Modeling Approach to Galaxy Clustering. *arXiv* (2022).
42. E Cameron, AN Pettitt, Approximate Bayesian Computation for astronomical model analysis: A case study in galaxy demographics and morphological transformation at high redshift. *Mon. Notices Royal Astron. Soc.* **425**, 44–65 (2012).
43. A Weyant, C Schafer, WM Wood-Vasey, Likelihood-free Cosmological Inference with Type Ia Supernovae: Approximate Bayesian Computation for a Complete Treatment of Uncertainty. *The Astrophys. J.* **764**, 116 (2013).
44. C Hahn, et al., Approximate Bayesian Computation in Large Scale Structure: Constraining the galaxy-halo connection. *Mon. Notices Royal Astron. Soc.* **469**, 2791–2805 (2017).
45. D Huppenkothen, M Bachetti, Accurate X-ray Timing in the Presence of Systematic Biases With Simulation-Based Inference (2021).
46. K Zhang, et al., Real-time Likelihood-free Inference of Roman Binary Microlensing Events with Amortized Neural Posterior Estimation. *Astron. J.* **161**, 262 (2021).
47. C Hahn, P Melchior, Accelerated Bayesian SED Modeling using Amortized Neural Posterior Estimation (2022).
48. EG Tabak, E Vanden-Eijnden, Density estimation by dual ascent of the log-likelihood. *Commun. Math. Sci.* **8**, 217–233 (2010).
49. EG Tabak, CV Turner, A Family of Nonparametric Density Estimation Algorithms. *Commun. on Pure Appl. Math.* **66**, 145–164 (2013).
50. F Villaescusa-Navarro, et al., The Quijote Simulations. *The Astrophys. J. Suppl. Ser.* **250**, 2 (2020).
51. PS Behroozi, RH Wechsler, HY Wu, The ROCKSTAR Phase-space Temporal Halo Finder and the Velocity Offsets of Cluster Cores. *The Astrophys. J.* **762**, 109 (2013).
52. A Knebe, et al., Haloes gone MAD: The Halo-Finder Comparison Project. *Mon. Notices Royal Astron. Soc.* **415**, 2293–2318 (2011).
53. Z Zheng, AL Coil, I Zehavi, Galaxy Evolution from Halo Occupation Distribution Modeling of DEEP2 and SDSS Galaxy Clustering. *The Astrophys. J.* **667**, 760–779 (2007).
54. AR Zentner, A Hearin, FC van den Bosch, JU Lange, A Villarreal, Constraints on Assembly Bias from Galaxy Clustering. *arXiv:1606.07817 [astro-ph]* (2016).
55. M Vakili, C Hahn, How Are Galaxies Assigned to Halos? Searching for Assembly Bias in the SDSS Galaxy Clustering. *The Astrophys. J.* **872**, 115 (2019).
56. B Hadzhiyska, et al., Galaxy assembly bias and large-scale distribution: A comparison between IllustrisTNG and a semi-analytic model. *Mon. Notices Royal Astron. Soc.* **508**, 698–718 (2021).
57. J Carlson, M White, Embedding realistic surveys in simulations through volume remapping. *The Astrophys. J. Suppl. Ser.* **190**, 311–314 (2010).
58. Planck Collaboration, et al., Planck 2018 results. VI. Cosmological parameters. *arXiv:1807.06209 [astro-ph]* (2018).
59. N Hand, Y Li, Z Slepian, U Seljak, An optimal FFT-based anisotropic power spectrum estimator. *J. Cosmol. Astro-Particle Phys.* **07**, 002 (2017).
60. B Uria, MA Côté, K Gregor, I Murray, H Larochele, Neural Autoregressive Distribution Estimation. *arXiv:1605.02226 [cs]* (2016).
61. DS Greenberg, M Nonnenmacher, JH Macke, Automatic Posterior Transformation for Likelihood-Free Inference (2019).
62. A Tejero-Cantero, et al., Sbi: A toolkit for simulation-based inference. *J. Open Source Softw.* **5**, 2505 (2020).
63. DP Kingma, J Ba, Adam: A Method for Stochastic Optimization. *arXiv:1412.6980 [cs]* (2017).
64. B Dey, et al., Calibrated Predictive Distributions via Diagnostics for Conditional Coverage (2022).
65. D Zhao, N Dalmaso, R Izbicki, AB Lee, Diagnostics for conditional density models and Bayesian inference algorithms in *Proceedings of the Thirty-Seventh Conference on Uncertainty in Artificial Intelligence*. (PMLR), pp. 1830–1840 (2021).
66. M Cacciato, FC van den Bosch, S More, H Mo, X Yang, Cosmological constraints from a combination of galaxy clustering and lensing - III. Application to SDSS data. *Mon. Notices Royal Astron. Soc.* **430**, 767–786 (2013).
67. R Mandelbaum, et al., Cosmological parameter constraints from galaxy-galaxy lensing and galaxy clustering with the SDSS DR7. *Mon. Notices Royal Astron. Soc.* **432**, 1544–1575 (2013).
68. A Leauthaud, et al., Lensing is low: Cosmology, galaxy formation or new physics? *Mon. Notices Royal Astron. Soc.* **467**, 3024–3047 (2017).
69. C Hikage, et al., Cosmology from cosmic shear power spectra with Subaru Hyper Suprime-Cam first-year data. *Publ. Astron. Soc. Jpn.* **71**, 43 (2019).
70. M Asgari, et al., KIDS-1000 cosmology: Cosmic shear constraints and comparison between two point statistics. *Astron. & Astrophys. Vol. 645, id.A104, <NUMPAGES> 31 </NUMPAGES> pp. 645, A104* (2021).
71. A Krolewski, S Ferraro, M White, Cosmological constraints from unWISE and Planck CMB lensing tomography. *J. Cosmol. Astropart. Phys.* **2021**, 028 (2021).
72. A Amon, et al., Dark Energy Survey Year 3 results: Cosmology from cosmic shear and robustness to data calibration. *Phys. Rev. D* **105**, 023514 (2022).
73. JU Lange, et al., Five per cent measurements of the growth rate from simulation-based modelling of redshift-space clustering in BOSS LOWZ. *Mon. Notices Royal Astron. Soc.* **509**, 1779–1804 (2022).
74. PD Meerburg, Alleviating the tension at low l through axion monodromy. *Phys. Rev. D* **90**, 063529 (2014).
75. A Chudaykin, D Gorbuonov, I Tkachev, Dark matter component decaying after recombination: Sensitivity to baryon acoustic oscillation and redshift space distortion probes. *Phys. Rev. D* **97**, 083508 (2018).
76. E Di Valentino, A Melchiorri, O Mena, S Vagnozzi, Nonminimal dark sector physics and cosmological tensions. *Phys. Rev. D* **101**, 063502 (2020).
77. GF Abellán, R Murgia, V Poulin, J Laval, Implications of the S8 tension for decaying dark matter with warm decay products. *Phys. Rev. D* **105**, 063525 (2022).
78. H Gil-Marín, et al., The clustering of galaxies in the SDSS-III Baryon Oscillation Spectroscopic Survey: RSD measurement from the power spectrum and bispectrum of the DR12 BOSS galaxies. *Mon. Notices Royal Astron. Soc.* **465**, 1757–1788 (2017).
79. B Reid, et al., SDSS-III Baryon Oscillation Spectroscopic Survey Data Release 12: Galaxy target selection and large-scale structure catalogues. *Mon. Notices Royal Astron. Soc.* **455**, 1553–1573 (2016).